ACS APPLIED MATERIALS & INTERFACES

www.acsami.org

Research Article

Silver Nano-Inks Synthesized with Biobased Polymers for High-Resolution Electrohydrodynamic Printing Toward In-Space Manufacturing

Tyler Kirscht,[1] Liangkui Jiang,[1] Fei Liu, Xuepeng Jiang, Matthew Marander, Ricardo Ortega, Hantang Qin,* and Shan Jiang*

Cite This: https://doi.org/10.1021/acsami.4c07592

Read Online

ACCESS | Metrics & More | Article Recommendations | Supporting Information

ABSTRACT: Electrohydrodynamic (EHD) printing is an additive manufacturing technique capable of producing micro/nanoscale features by precisely jetting ink under an electric field. However, as a new technique compared to more conventional methods, commercially available inks designed and optimized for EHD are currently very limited. To address this challenge, a new silver nanoink platform was developed by synthesizing silver nanoparticles *in situ* with biobased polymer 2-hydroxyethyl cellulose (HEC). Typically used as a thickening agent, HEC is cost-effect, biocompatible, and versatile in developing inks that meet the rheology criteria for high-resolution EHD jetting. This approach significantly outperforms the traditional use of polyvinylpyrrolidone (PVP), enabling the stabilization of high solids content (>50 wt %) nanoinks for over 10 months with an HEC dosage 20 times lower than that required by PVP. The HEC-synthesized silver ink displays excellent electrical properties, yielding resistivities as low as 2.81 $\mu\Omega$ cm upon sintering, less than twice that of pure silver. Additionally, the capability to sinter at low temperatures (<200 °C) enables the use of this ink on polymer substrates for flexible devices. The synthesized nanoinks were also found to be capable of producing precise, high-resolution features by EHD printing with smooth lines narrower than 5 μm printed using a 100 μm nozzle. Additionally, a semiempirical model was developed to reveal the relationship between printing resolution, ink properties, and printing parameters, enabling precise printing control. Moreover, for the first time, the unique ability of EHD to achieve precise fabrication under microgravity was conclusively demonstrated through a parabolic flight test utilizing the HEC-based nanoinks. The study greatly expands the potential of printing thin films for the on-demand manufacturing of electronic devices in space.

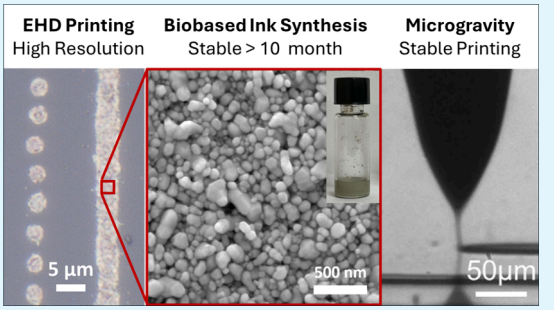

KEYWORDS: *silver nanoink, conductive ink, electrohydrodynamic printing, in-space manufacturing, microelectronics*

1. INTRODUCTION

Additive manufacturing has seen a rise in popularity in recent years as a technique to fabricate electronic devices. However, it is still very challenging to achieve fine features on the micron scale with the conventional printing methods. Electrohydrodynamic (EHD) printing can help address the challenge by utilizing a strong electric field to jet inks into very fine droplets (<1 pl volumes).[1] A high voltage is applied between the printing nozzle and substrate, which pulls the ink and forms a "Taylor cone" at the nozzle tip due to the equilibrium of electric and capillary forces.[2] This allows for the printing of features much smaller than the opening of the nozzle.[3] The capability of printing such high-resolution features (<10 μm) is one of the biggest advantages of EHD printing when compared to other techniques such as conventional inkjet, aerosol jet, or screen printing.[4] Therefore, EHD can be used to produce thin films and fabricate smaller and more compact devices.

Another advantage of EHD is that it is capable of printing inks with a wide range of viscosities (1−1000 mPa s)[5] and even pastes exceeding 20 000 mPa s.[6] In comparison, conventional inkjet printing requires ink with much lower viscosities, typically in the range of 1−10 mPa s.[7] On the other hand, printing behavior is highly dependent on ink viscosity. While EHD is capable of printing commercially available inks in the lower viscosity range, it is not ideal for achieving smooth and high-resolution printing. Ultrafine nozzle tips with openings close to the size of the printed features are often utilized, which diminishes the advantage of the Taylor cone effect.[8] Additionally, such small nozzles are more difficult and costly to produce and tend to be more fragile and likely to clog during printing.[9] Higher viscosity (non-Newtonian) inks, on

Received: May 9, 2024
Revised: July 11, 2024
Accepted: July 15, 2024

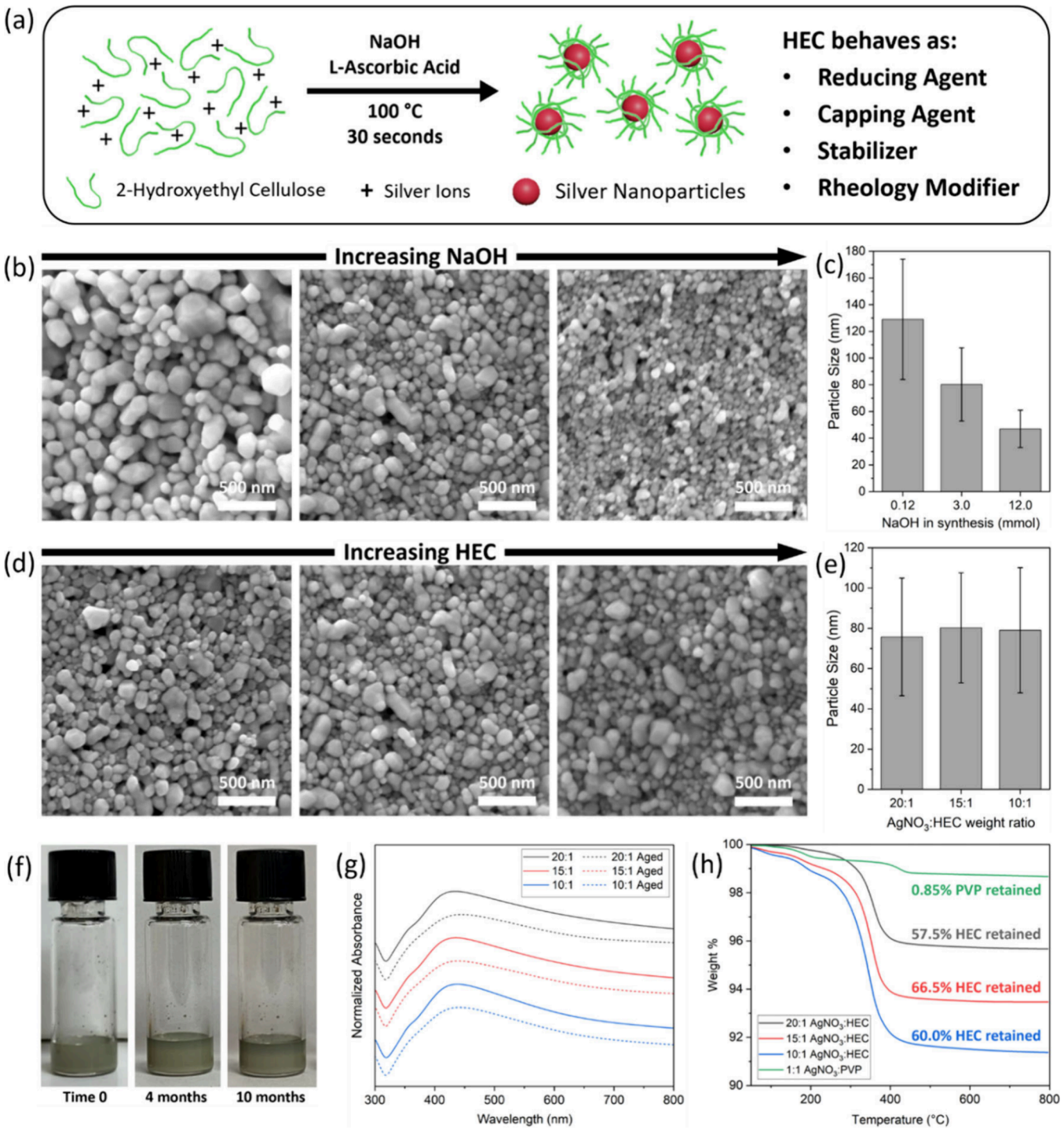

Figure 1. (a) Schematic of silver nanoink synthesis using HEC. (b) SEM images of AgNPs synthesized with increasing NaOH. (c) Particle sizes of AgNPs synthesized with increasing NaOH. (d) SEM images of AgNPs synthesized with increasing HEC. (e) Particle sizes of AgNPs synthesized with increasing HEC. (f) Images of 10:1 silver ink aged over 10 months. (g) UV−vis spectra of silver inks before and after accelerated aging. (h) Thermogravimetric analysis of silver nanoparticles synthesized with HEC and PVP after washing.

the other hand, have been shown to lead to more stable jets in the EHD process.[10] Given that EHD is a newer, less utilized technique, there is currently a very limited selection of commercial inks that have been designed or optimized for high-resolution EHD printing.

The advantages of EHD printing also enable its use for precise fabrication in distinctive scenarios, such as manufacturing in space, where gravity is absent.[11] Because the electric field is the dominant force for controlling material jetting in EHD printing, there is little reliance on gravitational forces for printing.[12] For this reason, the technique has drawn interest from NASA for use in outer space missions.[13] For such an application, it is crucial to have inks optimized for the printing technique. Given the limited accessibility of resources in the isolated environment of a space station, it is necessary that the inks remain highly stable over a long shelf life. It is also preferred to use larger, more robust nozzles for printing to reduce the likelihood of breaking or clogging while still

https://doi.org/10.1021/acsami.4c07592
ACS Appl. Mater. Interfaces XXXX, XXX, XXX−XXX

maintaining the ability to produce high-resolution features. Furthermore, without knowing the detailed composition of commercial inks, very little can be done to correlate the printing behaviors with the ink compositions and properties. Therefore, we developed our own silver nanoink platform, which allows us to fully control the ink compositions and properties and optimize them for EHD printing.

Of the materials that may be used in the fabrication of electronic devices, silver is most ideal for the printing of conductive electrodes due to having both excellent electrical conductivity and resistance to oxidation.[14] Printable silver inks often consist of silver nanoparticles (AgNPs) suspended in a colloidal solution. These nanoparticles are typically synthesized in the presence of an organic capping/stabilizing agent to control the particle size and keep them stable in suspension. By far, the most commonly used stabilizing agent in silver nanoparticle inks is polyvinylpyrrolidone (PVP).[15−23] The stability of the nanoparticles is important not only to provide a long shelf life but also to ensure the nozzle will not be clogged during the printing process. In order to improve the stability, an excess amount of stabilizing agent usually has to be added to the nanoparticle suspension. In addition, the nanoinks are often formulated with a rheology modifier and other reagents to assist the printing. These organic components added to the ink formulation may increase the required sintering temperature or lower the conductivity. It is highly desirable to develop a highly stable silver nanoink with a low amount of organic compounds, low sintering temperature, and high conductivity.

In this work, we present a new nanoink platform synthesized *in situ* with a biobased polymer, 2-hydroxyethyl cellulose (HEC), to be used in high-resolution EHD printing. HEC is already widely used in industry as a thickening agent and can induce a very steep shear-thinning rheology profile.[24−26] This is relevant as ink viscosity considerations are very important for EHD printing. As a derivative of cellulose, HEC is also easily renewable and biocompatible. Additionally, HEC is very cost-effective, priced at about half that of PVP in bulk. These attributes make it a promising candidate for use in synthesizing silver nanoinks. HEC has previously been shown as an effective reducing and stabilizing agent in the synthesis of silver nanoparticles;[27,28] however, in these cases, the nanoparticles were not tested for their electrical properties. Additionally, the HEC was used in significant excess compared to the silver precursor, and the silver concentration was very low. As such, the resulting suspensions would likely not be suitable for conductive inks, as the high organic content would inhibit the flow of electric current. The literature of utilizing HEC as a reagent for synthesizing functional nanoinks is very limited, especially for highly concentrated silver nanoparticle inks (∼50 wt %) made for EHD printing.

In our synthesis, HEC was utilized with multiple functionalities, including as a reducing agent, capping agent, dispersant, and rheology modifier. This helps to significantly simplify our formulations. In addition, we systematically investigated the synthetic conditions that lead to HEC silver nanoinks of different properties and studied the printing behaviors of these nanoinks with an EHD printer. We discovered that silver nanoinks synthesized with HEC displayed great electrical properties and showed superior stability at a much lower stabilizer dose compared to PVP. Moreover, we have developed a model that establishes a correlation between ink properties and printing performance, providing a methodology for predicting and tuning the behavior of EHD printing with these nanoinks in future applications, including for use in in-space manufacturing. As a proof of concept, for the first time, we successfully printed precise patterns under microgravity using an EHD printer with the HEC nanoinks in a very challenging environment during a parabolic flight test. The results open the opportunity of utilizing an EHD for future on-demand fabrication of devices in space.

2. RESULTS AND DISCUSSION

2.1. Synthesis of Silver Nanoinks. Silver nanoparticles were synthesized using silver nitrate as a silver precursor *in situ* with biobased polymer 2-hydroxyethyl cellulose (HEC) as a reducing agent, capping agent, and stabilizer as outlined in Figure 1a. L-Ascorbic acid was also added to boost the reducing power, and sodium hydroxide was used to tune the pH of the synthesis. It was discovered that increasing the sodium hydroxide content of the synthesis leads to smaller and more monodisperse nanoparticles, ranging between 129.0 ± 45.2 and 47.4 ± 13.7 nm for a NaOH content of 0.12 and 12.0 mmol, respectively, as seen under SEM in Figures 1b,c. This trend is consistent with the findings of Qin et al., who used citrate as the stabilizer for silver nanoparticle synthesis, although the precursor and reducing agent concentrations are completely different.[29] With NaOH held constant at 3.0 mmol, samples were synthesized with three different $AgNO_3$/HEC weight ratios: 20:1, 15:1, and 10:1. Any ratio with a HEC content lower than 20:1 was found to result in flocculation of nanoparticles upon reduction of the silver. These samples have average particle sizes of 75.8 ± 29.2 nm, 80.2 ± 27.3 nm, and 79.0 ± 31.1 nm, respectively (Figures 1d,e). This indicates that the amount of HEC used in the synthesis has no significant effect on the resulting nanoparticle size. This differs with the findings of works using polyvinylpyrrolidone (PVP) as the capping agent/stabilizer, in which increasing the amount of PVP with respect to the silver precursor has been shown to cause a decrease in particle size.[15−17]

The new synthetic approach is highly efficient in terms of both the reaction time and productivity rate. The whole reaction completes within 1 min with a ∼100% yield. Samples of 20:1, 15:1, and 10:1 silver nanoparticles were washed and separated out with ethanol and acetone in two cycles, and the supernatant was tested for remaining Ag^+ ions by adding NaCl solution dropwise. The lack of AgCl precipitate forming indicated that there were no remaining Ag^+ ions, and the reaction produced 100% yield. The particles were dispersed in dimethyl sulfoxide (DMSO) at 50 wt % loading to formulate the inks. DMSO is an organic solvent with a high boiling point at 189 °C. This ensures that the inks do not dry too quickly while printing and clog the printing nozzle. The nanoparticle suspensions remained highly colloidally stable, with no visible signs of flocculation after several months of storage. Figure 1f shows images of a stable 10:1 sample over 10 months of natural aging. The stability of the inks was also tested by measuring the absorbance of the particles before and after accelerated aging. Repeat samples were prepared and placed in an oven set to 60 °C for a heat age of 21 days, which equates to an age of 9 months at 23 °C per ASTM F1980. Figure 1g shows the normalized UV−vis spectra recorded before and after aging for each ink. For each sample, the curves maintain a similar shape and do not show any shifts in peak absorbance wavelength. This indicates that the nanoparticles remained colloidally stable under the aging conditions.

https://doi.org/10.1021/acsami.4c07592
ACS Appl. Mater. Interfaces XXXX, XXX, XXX−XXX

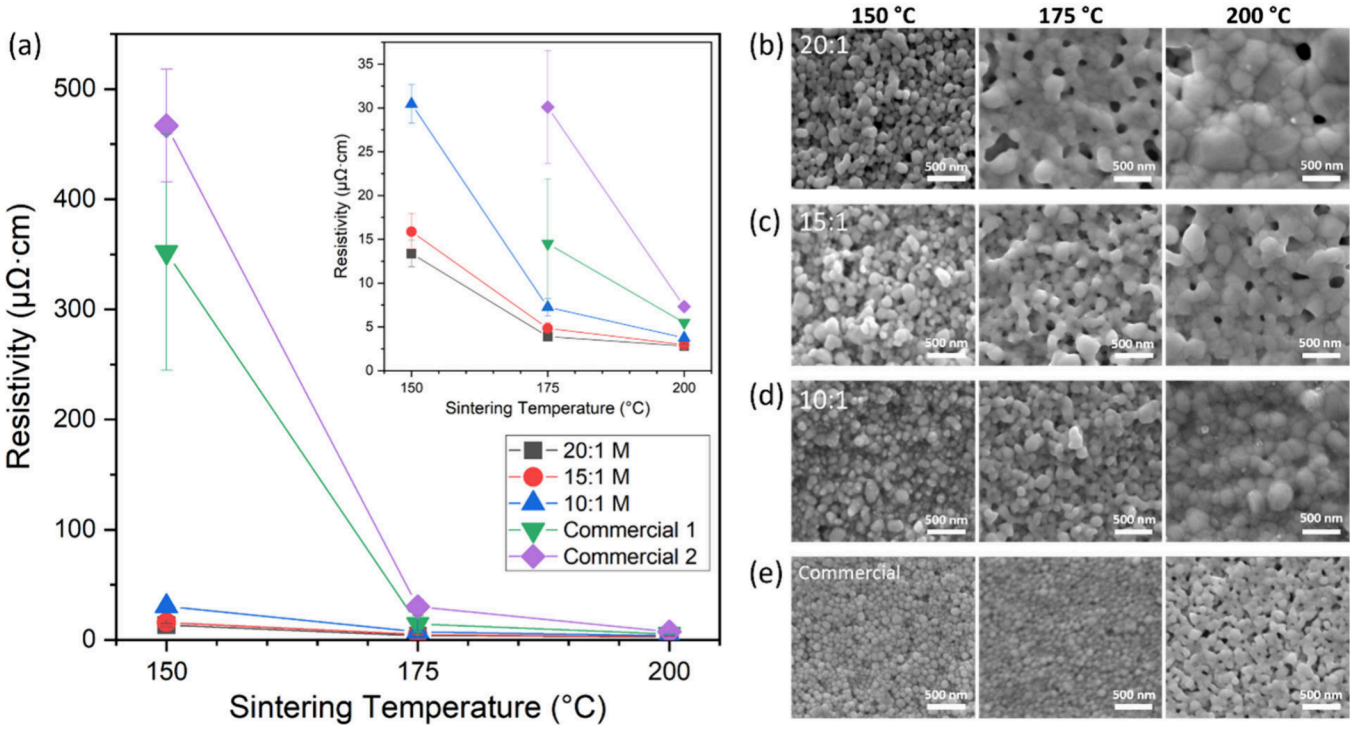

Figure 2. (a) Resistivities of synthesized and commercial silver inks after sintering at 150 °C, 175 °C, and 200 °C for 30 min. SEM images of films of (b) 20:1, (c) 15:1, (d) 10:1, and (e) commercial inks sintered at 150 °C, 175 °C, and 200 °C for 30 min.

To assess the scalability of the new HEC-based synthesis method, a large-scale synthesis containing 10× the amount of each reagent was performed with a 20:1 $AgNO_3$/HEC ratio. The reaction resulted in nanoparticles with an average size of 82.1 ± 25.9 nm (Figure S1), very similar to those synthesized on the typical scale. When dispersed in DMSO, the resulting ink remains highly stable and shows no apparent differences compared to the typical 20:1 ink, indicating excellent scalability for this synthesis method. As a comparison to the *in situ* method, HEC was also directly formulated with commercially purchased silver nanoparticles; however, this approach was not found to yield any stable nanoinks, highlighting the importance of HEC as a capping agent in the synthesis. In addition to silver, the use of HEC was explored for the synthesis of nanoinks of other materials, including copper, barium titanate, and tungsten oxide. Preliminary results are shown in Figure S2.

The effectiveness of HEC as a stabilizer for silver nanoparticles is also evidenced by its high degree of retention through processing of the ink. Thermogravimetric analysis (TGA) was performed on dried deposits of the inks to determine the amount of organic material in the solids content (Figure 1h). When ramped to 800 °C, 20:1, 15:1, and 10:1 inks were found to have mass losses of 4.33%, 6.53%, and 8.63%, respectively. The majority of mass loss occurred between 250 and 400 °C for each sample. This is consistent with the TGA curve for pure HEC powder, which was found to have over 90% mass loss when ramped to 800 °C (Figure S3). By comparing the weight ratio of metal to organic content in the inks' solids to that of $AgNO_3$/HEC in the synthesis for each sample, and knowing that 100% of the silver is reduced, it is calculated that an average of 61.3 ± 4.7% of the HEC used is retained through two washing cycles for the three samples. This indicates that HEC bonds very strongly to the silver surface, making it a very efficient stabilizing agent. This is most likely due to an abundance of functional groups along the HEC polymer chain, which contains three per repeating unit. These include reactive hydroxyl groups as well as some aldehyde groups, while the formation of new aldehyde groups is promoted by the oxidation degradation of HEC under basic conditions (pH 12 or above) at reaction temperatures above 70 °C. El-Sheikh et al. previously displayed the interaction between silver and HEC through Fourier transform infrared (FTIR) measurements, confirming the interaction of both hydroxyl and aldehyde groups in the reduction of silver ions and stabilization of the resulting silver nanoparticles.[27]

A direct side-by-side comparison suggests that HEC markedly outperforms PVP in both efficacy and stability. In a control experiment, silver nanoparticles were synthesized using the same procedure but replacing HEC with PVP as the capping agent and stabilizer. It was also necessary to adjust the amount of NaOH used to achieve particles of a size similar to those synthesized with HEC (Figure S4). The PVP-synthesized nanoparticles were not found to be colloidally stable after washing and formulating into an ink when using PVP content lower than a 1:1 weight ratio with silver nitrate. Using TGA, it was found that the solids for this sample contained only 1.33% organic content after just one wash cycle, corresponding to a 0.85% retention of the PVP used in the synthesis (Figure 1h). That is more than 60 times lower retention than HEC. This also displays a unique advantage of using HEC as a stabilizer. Due to its high capping efficiency, far less of it can be used when compared to other stabilizing agents such as PVP, saving on cost and material waste. It is typical in other works for PVP to be used in a near 1:1 weight ratio or even exceeding the amount of silver nitrate in the synthesis of silver nanoinks when following a similar one-step reduction process.[18−23] Meanwhile, HEC is able to effectively

https://doi.org/10.1021/acsami.4c07592
ACS Appl. Mater. Interfaces XXXX, XXX, XXX−XXX

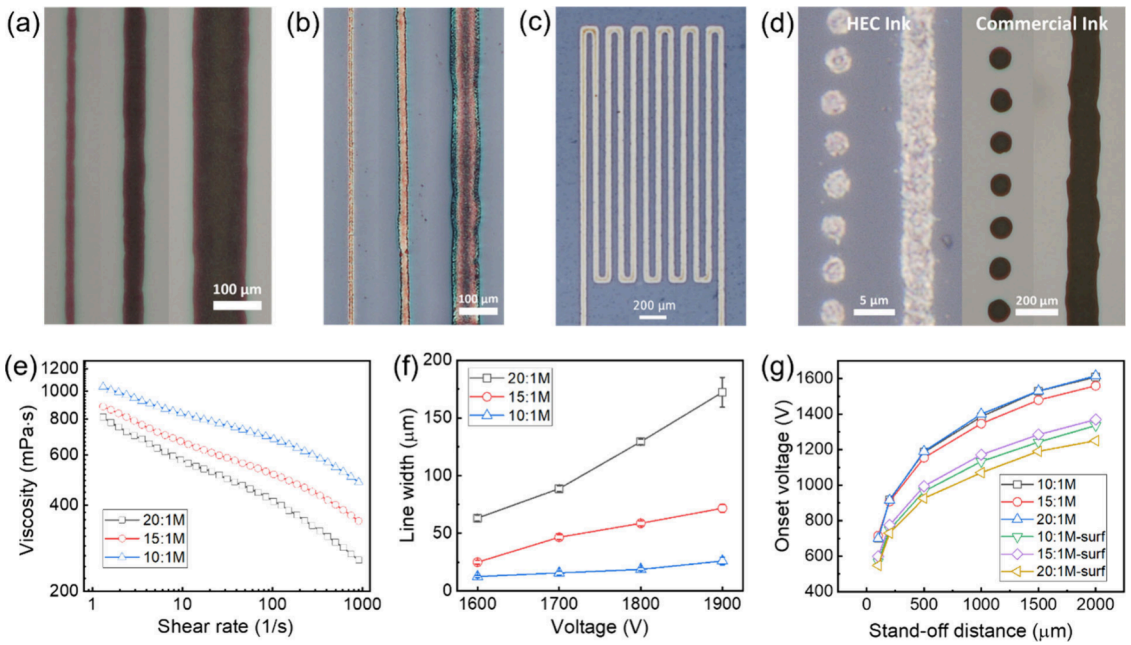

Figure 3. (a) Fresh ink and (b) 10-months aged ink EHD printed at different line widths by varying printing speed. (c) Test pattern printed with synthesized ink. (d) Highest resolution EHD printing of dots and lines with the HEC-synthesized ink (left) compared to commercial silver ink (right). (e) Rheology profiles of inks with varying HEC amounts. (f) Printed line widths of inks with varying HEC amounts under increasing voltage. (g) Onset voltage of inks with and without surfactant at different stand-off distances.

stabilize silver nanoparticles using 20× smaller quantities. When also considering HEC's low cost and biocompatibility, it makes for a very advantageous alternative.

2.2. Electrical Performance. In order to obtain high conductivity for printed patterns with metallic nanoink, a sintering step is necessary. Upon deposition, the particles are coated with the organic stabilizing agent, which behaves as a natural insulator, inhibiting the flow of electrical current between particles. A sintering step can remove this insulating layer while also fusing particles together through diffusion at the particle surfaces in contact, creating a continuous pathway for electron flow through the metal. To benchmark the sintering performance, we carefully compared the resistivity of HEC nanoinks with commercial inks prepared under similar conditions.

Dried films of 20:1, 15:1, and 10:1 inks were sintered at 150 °C, 175 °C, and 200 °C for 30 min each, and the resistivities were measured, shown in Figure 2a. All inks showed excellent electrical performance, with the 20:1 ink achieving a resistivity of 2.81 $\mu\Omega$ cm when sintered at 200 °C, less than twice the resistivity of pure silver (1.59 $\mu\Omega$ cm). It also showed very good conductivity at 150 °C sintering with a resistivity of 13.38 $\mu\Omega$ cm, making it useful for applications where a high sintering temperature cannot be used. This would include electronics printed on flexible polymeric substrates such as PET, which may experience damage when exposed to temperatures above 200 °C.[30] For a comparison, commercially available silver nanoinks were purchased from two reputable companies, and their resistivities were measured under the same conditions. Commercial ink 1 (Sigma-Aldrich 796042) contains 50 wt % Ag in tripropylene glycol monomethyl ether, and commercial ink 2 (Novacentrix JS-A191) contains 40 wt % Ag in aqueous suspension. Upon sintering, all three synthesized HEC inks outperformed both commercial inks at all sintering temperatures but especially so at 150 °C, where both commercial inks displayed average resistivities over 350 $\mu\Omega$ cm.

It can also be seen in Figure 2a that the inks follow a trend of having lower resistivity when containing less HEC at all temperatures. This is directly reflected by the sintering action observed in SEM images of the topographies of the films shown in Figure 2b–d. Sintering action can be observed in the 20:1 sample at 150 °C through the initial joining of particles, while this is not apparent in the other two samples. At 175 °C, there is a very high degree of particle sintering for sample 20:1 as the original size and shape of the particles are no longer distinguishable, instead forming a continuous mass. This is also observed to a lesser degree in sample 15:1, while very little of this is seen in sample 10:1. At 200 °C, all three samples show significant fusion, allowing for uninhibited electron flow. This trend makes sense, as it takes longer to sinter away higher amounts of the organic coating that protects the particles. Figure 2e shows the topographies of sintered films of commercial ink 1, which does not show any particle fusion until 200 °C, and even then, it is more porous and less well-connected than any of the synthesized inks.

The high conductivity of the HEC inks, especially at the lower sintering temperatures, may be in part due to the low content of the organic stabilizer as well as the low degradation temperature of HEC compared to alternatives such as PVP. While HEC begins to degrade just above 200 °C, PVP does not do so until around 400 °C as shown by the TGA curves in Figure S3. As such, the sintering behavior of the silver nanoparticles benefits from a more rapid removal of the protective and insulating coating as the sintering temperature approaches the organic degradation temperature. The TGA curve for HEC also indicates that some byproduct of HEC (~30 wt %) may remain after initial degradation. This, however, does not appear to have a negative effect on the electrical property of the sintered film, as the conductivity approaches that of pure silver.

To assess the potential for usage in flexible electronics, a 2 cm line of the synthesized ink (15:1) was printed on a strip of

https://doi.org/10.1021/acsami.4c07592
ACS Appl. Mater. Interfaces XXXX, XXX, XXX−XXX

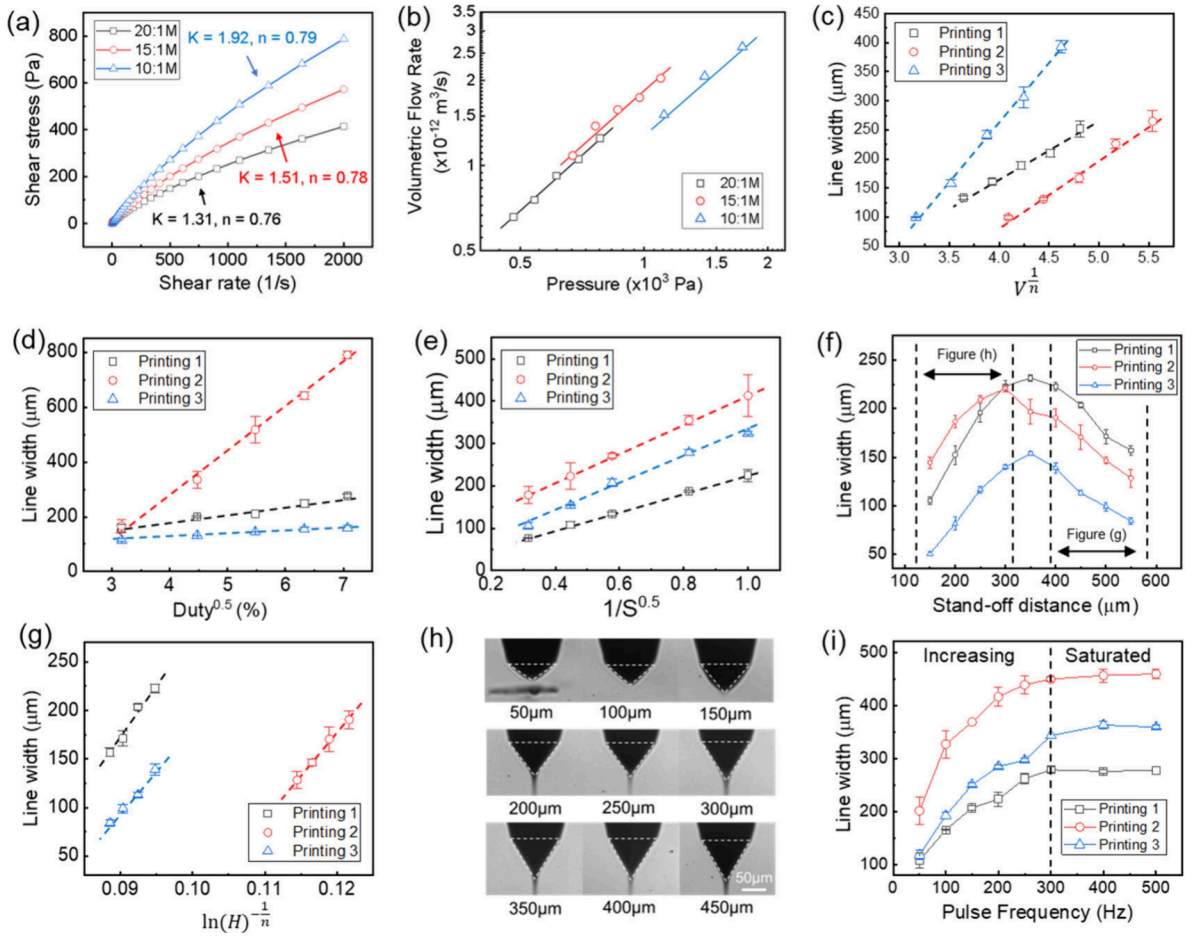

Figure 4. (a) Rheology model fitting of the inks. (b) Experimental validation for eq 1. (c–g) Validation of scaling law between line width and (c) applied voltage, (d) duty ratio, (e) printing speed, and (f,g) stand-off distance. (h) Conical shape of ink jetting at various stand-off distances. (i) Relationship between line width and pulse frequency.

polyimide and sintered at 200 °C for 30 min. The resistance across the line was measured using a multimeter with the substrate both flat and bent, as shown in Figure S5. The resistance displayed an increase from 272 to 277 Ω during bending, a change of just 1.8%, and full recovery was observed when flattened again. The adhesion of the ink to the flexible substrate was also evaluated using the crosshatch and tape-peel method outlined in ASTM F1842. Excellent adhesion was observed after sintering at all three temperatures, with no ink being pulled off the polyimide surface by the tape, as displayed in Figure S6. These properties along with the conductivity and sintering results indicate great potential for use of the HEC-synthesized ink in the fabrication of flexible devices.

2.3. Printing Performance. One of the biggest advantages of electrohydrodynamic printing is that it is capable of printing very high-resolution features (<10 μm), allowing for the production of highly compact electronic devices. The printing demonstration of the silver nanoink using EHD is shown in Figure 3. Using a nozzle with an opening diameter of 100 μm, the ink was found to print very smooth lines with widths ranging between 4 and 150 μm (Figure 3a). There are several ways that line width can be tuned in the EHD process, as outlined in section 2.4. In this case, the lines were made wider by slowing down the printing speed. The printing behavior was also tested with ink that had aged naturally for 10 months, as shown in Figure 3b. Smooth and consistent lines were still achieved, further indicating the high stability of the ink. A more complex printed test pattern is shown in Figure 3c. The pattern maintains consistent thickness across its entire length and, upon sintering, was found to be conductive from end-to-end. This shows that the ink maintains a highly stable jet over long stretches with multiple direction changes to create high-fidelity features, also indicating the high stability of the nanoparticle suspension under the electric field. A comparison of the highest-resolution features attained between our nanoink and a commercial silver ink (commercial ink 1) is shown in Figure 3d. Note that the change in color across the images is due to different lighting conditions of the microscopes used. Still using a nozzle with a diameter of 100 μm, our synthesized 20:1 ink was found to be capable of printing precise dots with average diameters 2.96 ± 0.25 μm and lines with average widths of 3.95 ± 0.44 μm when all printing parameters are optimized for high-resolution printing, over 25× smaller than the nozzle diameter. Meanwhile, even with optimization, the highest resolution features achieved by the commercial inkjet ink were dots with average diameters of 99.7 ± 2.4 μm and lines with average widths of 147.6 ± 1.6 μm, similar in size to the nozzle diameter and over 30× larger than the features printed with the synthesized HEC ink. The capability to achieve high-resolution EHD printing with a very similar commercial ink (same supplier and constitution, 30 wt % Ag loading) has been demonstrated by Yang et al.; however, in

https://doi.org/10.1021/acsami.4c07592
ACS Appl. Mater. Interfaces XXXX, XXX, XXX−XXX

this study, a superfine nozzle with an opening diameter of 1.8 μm was used to achieve printed line widths between 5 and 20 μm.[8] The capability of printing such fine features using a larger nozzle diameter presents several advantages. It diminishes the need for manufacturing more costly, more fragile, and smaller-diameter nozzles for high-resolution printing, minimizing the issue of nozzle clogging associated with small openings and reducing the likelihood of breaking the nozzle during operation. Additionally, it facilitates the use of ink formulations with higher loadings, enhancing the overall printing efficiency. And, as demonstrated, it still allows for larger features on the scale of the nozzle size to be printed, adding much versatility to the printing process without changing the nozzle.

The effect of the ink properties on the printing behavior was further studied by controlling the viscosity and surface tension. Rheology profiles of the inks were taken under increasing shear at 25 °C, shown in Figure 3e. All samples displayed significant shear thinning behavior, which is consistent with the literature for HEC-based formulations.[25,26] When increasing the HEC amount from 20:1 to 10:1, the viscosity increased from 257 to 482 mPa s at a shear rate of 1000 s^{-1}, demonstrating an effective and convenient method to control the ink viscosity in the HEC system. As shown in Figure 3f, printing inks with higher viscosity resulted in a higher resolution of the printed trace when all other factors were kept constant. This trend is consistent with previous works which have displayed that higher viscosity inks lead to smaller ejection volume of jetted drops in the EHD process.[31] The commercial ink, by contrast, has a viscosity of only around 10 mPa s, explaining its inability to print such high-resolution features. Additionally, inks in this low viscosity range are more likely to spread out upon deposition, further increasing the line width. Figure 3f also displays the effect of increasing printing voltage on printed line width, where wider lines can be achieved with a higher printing voltage. To study the effects of ink surface tension, Triton X-45 surfactant was added to the inks at 1 wt %, and the printing behavior was compared to that without the addition. Figure 3g shows the onset voltage of inks with and without a surfactant at various stand-off distances (the distance between the nozzle tip and the substrate). Onset voltage is the minimum voltage that maintains a stable cone-jet status in EHD inkjet printing. As standoff distance increases, the onset voltage was found to also increase. By adding surfactant, the onset voltage for each ink was found to decrease at all stand-off distances, indicating a lower barrier to generate the EHD phenomenon and potential to control the jetting process more easily.

2.4. Printing Behavior Model. The EHD printing process is influenced by various factors, including the geometry (such as nozzle size and shape), operation parameters (such as voltage), and ink properties (such as surface tension and viscosity). Our focus is on the operation parameters, which are commonly used for EHD printing optimization, as they can be easily adjusted during the process. These include the back pressure, voltage amplitude, voltage frequency, duty ratio for pulse signals, plotting speed, and stand-off distance. A semiquantitative model has been established to better understand the printing behavior and control the printing process. The effect of the operation parameters on the printed line width was studied based on both physics and experimental results. It is important to note that the optimal range of parameters can vary depending on the type of ink used. Therefore, the parameter ranges for the printing tests differed to accommodate different inks. Figure 4a presents the trend of shear stress with the change in the shear rate for all three inks with different HEC amounts. It clearly indicates a non-Newtonian power-law behavior for all inks. For the following model, power-law coefficients K and n were calculated by fitting the rheology curves. Additionally, with the presence of silver nanoparticles, the conductivity of the suspension is larger than 10^{-5} S m^{-1}. For "high conductivity" liquids (>10^{-5} S/m) at length scales of hundreds of microns, the relationship among transport process time scale (τ_P), the charge relaxation time (τ_C), and the magnetic characteristic time (τ_M) is given by $\tau_P > \tau_C \gg \tau_M$.[32] Under these conditions, the jetting pulsation can be considered quasi-steady. As a result, the charge distribution can be seen as uniform throughout the process, and the effect of conductivity is not considered in the model.[33] The drop formation rate is therefore controlled by the balance of forces exerted on the liquid, including electric stress of repelling ions at the air/liquid interface, viscous stress, and capillary stress. Given the length and the diameter of the nozzle, for a laminar flow, the volumetric flow rate can be estimated by eq 1:[34,35]

$$Q = \frac{\pi R^3}{\frac{1}{n} + 3}\left[\frac{R}{2LK}\left(\frac{\varepsilon_0 {E_0}^2}{2} - \frac{\gamma}{R} + \Delta P\right)\right]^{1/n} \quad (1)$$

where Q is the volumetric flow rate (unit: m^3 s^{-1}), R is the radius of the nozzle (unit: m), L is the nozzle length (unit: m), K and n are the coefficients for the power law fit from the rheological profiles, ε_0 is the vacuum permittivity (unit: F m^{-1}), E_0 is the electrical field intensity (unit: V m^{-1}), γ is surface tension of the liquid (unit: N m^{-1}), and ΔP is the back pressure (include hydrostatic pressure if gravity exist). The validation of the equation is shown in Figure 4b, which is the plot of volumetric flow rate as a function of the total stress (including electrical stress, capillary stress, and back pressure) on the logarithmic scale. The dots are the experimental results of three inks with different viscosities, and the lines are the theoretical results based on eq 1. The results showed an excellent match between the model and the experimental data, indicating a good accuracy of eq 1 for flow rate estimation. The electrical field in a typical EHD printing system can be simplified and modeled by a semi-infinite wire perpendicular to an infinite planar counter electrode, so the electrical field intensity can be estimated by eq 2:[36]

$$E = \frac{2V}{R \cdot \ln\left(\frac{4H}{R}\right)} \quad (2)$$

where E is the electrical field intensity (unit: V/m), V is the electrical potential applied to the nozzle (unit: V), R is the radius of the nozzle (unit: m), and H is the stand-off distance of the nozzle to the substrate (unit: m). Now we have obtained the equation for the flow rate estimation by using operating parameters, geometry parameters, and ink properties. The next step is to model the relationship between flow rate and the final printed trace. By assuming the liquid flow is steady and stable during the whole printing process and neglecting the effect of shrinking on the line width during the evaporation process of deposited liquid, the line width can be expressed by eq 3:[37]

$$w = \sqrt{\frac{Q \cdot D}{\nu \cdot \left(\frac{\theta}{4 \sin^2 \theta} - \frac{\cos \theta}{4 \sin \theta}\right)}} \quad (3)$$

https://doi.org/10.1021/acsami.4c07592
ACS Appl. Mater. Interfaces XXXX, XXX, XXX−XXX

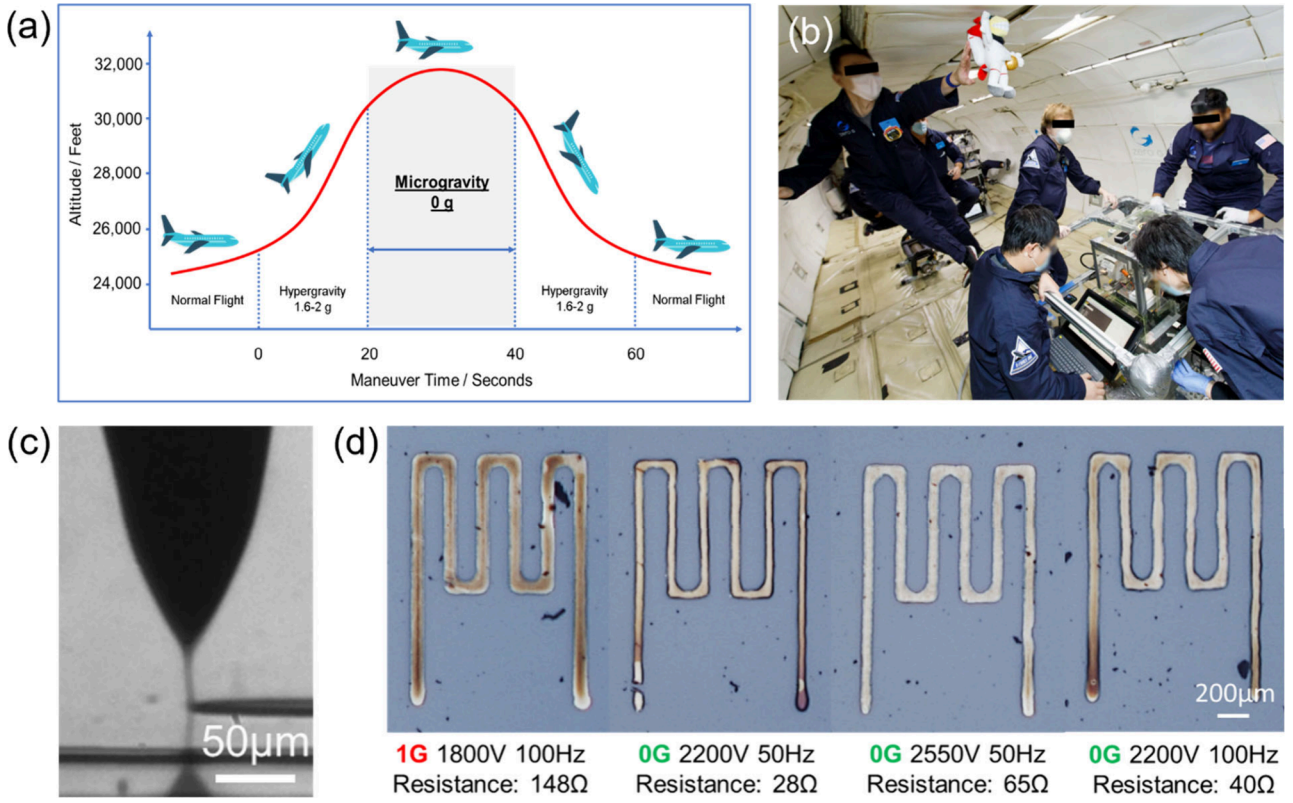

Figure 5. (a) Trajectory and gravitational changes for a parabolic flight cycle. (b) EHD printing experiments performed in microgravity. (c) A stable Taylor cone jet in microgravity. (d) Comparison of silver ink patterns printed with and without gravity.

where w is the line width of the final printed trace (unit: m), Q is the volumetric flow rate exiting the nozzle (unit: $m^3\ s^{-1}$), D is the duty cycle of the voltage signal (unit: %), v is the printing speed (unit: $m\ s^{-1}$), and θ is the contact angle between the droplet and the substrate. Combining eqs 1, 2, and 3, the scaling law between the printed line width of the final trace and the operation parameters can be achieved, displayed in eqs 4−7:

$$w \sim \sqrt{Q} \sim \sqrt[2n]{\Delta p} \sim \sqrt[2n]{\frac{1}{2}\varepsilon E^2} \sim V^{\frac{1}{2}} \tag{4}$$

$$w \sim D^{1/2} \tag{5}$$

$$w \sim \sqrt{Q} \sim \sqrt[2n]{\Delta p} \sim \sqrt[2n]{\frac{1}{2}\varepsilon E^2} \sim \ln(H)^{-1/n} \tag{6}$$

$$w \sim v^{-1/2} \tag{7}$$

A comprehensive derivation of the model presented is displayed in the Supporting Information. The derived scaling laws shown above were validated by experiments, as shown in Figure 4c−g. For each parameter, printing tests with three different inks were conducted. Surface tension and rheological coefficients for the inks are presented in Table S1. Three repetitions were done for each printing test. The model shows a good match to the experiments for the electrical potential (Figure 4c), duty cycle (Figure 4d), and printing speed (Figure 4e) through strong linear fits.

However, it is worth noting that the line width shows a nonmonotonic trend (increasing first, then decreasing) as the stand-off distance increases (Figure 4f). This is due to the constraint of the substrate to the cone jetting development in the EHD process. As shown in Figure 4h, it is clear that the conical shape was constrained by the substrate and cannot get fully developed when the stand-off distance is too small. With the stand-off distance increasing from 50 to 350 μm, the conical shape grows gradually and achieves full development. After the stand-off distance is higher than 350 μm, the effect of the stand-off distance on the line width can be predicted by the model accurately, as shown in Figure 4g. In terms of frequency, it can be divided into two stages: (1) when the frequency is relatively low, the line width will increase along with the frequency, and (2) the line width will no longer be affected after achieving a saturated point (300 Hz in this case), shown in Figure 4i.

In summary, we built a model to study the relationship between operating parameters and the printed line width, including electrical potential, duty cycle, frequency, printing speed, and stand-off distance. A good match was found between the model and the experiments, indicating that our model accurately captured the essential contributing factors. This model will offer a straightforward approach to establish a printing scheme for designing future printing processes under different conditions, including printing under microgravity.

2.5. Zero Gravity Experiments. One unique advantage of EHD printing is the ability to operate under zero gravity. Because the jetting mechanism utilizes electric forces and does not rely on gravity, we explored the potential of the technology for future in-space manufacturing under zero gravity sponsored by NASA. Given that electronic device failures are major malfunctions on the International Space Station (ISS), and resupply missions are very costly and infrequent, in-space additive manufacturing for electronics has been considered a top priority.[38] Additionally, fabricating sensors, such as air

https://doi.org/10.1021/acsami.4c07592
ACS Appl. Mater. Interfaces XXXX, XXX, XXX−XXX

quality monitoring and radiation exposure sensors, along with flexible printed electronics like power generators are nascent applications for the ISS.[39] In addition to the need for inks optimized for the EHD process, it was necessary to test the technique in a prolonged zero gravity environment to validate the potential for its use aboard the ISS.

For the first time, we successfully demonstrated the capability of printing precise patterns using EHD printing with HEC silver nanoinks under microgravity through a parabolic flight test. Figure 5a shows the trajectory and gravitational changes during a parabolic flight, which is capable of providing roughly 20 s bursts of microgravity. The gravitational changes were recorded during the flight using an accelerometer. Figure S7 shows steady periods of 17 s in which zero-gravity is observed. Figure 5b shows the printer operation and working environment during a period of microgravity. In this environment, the electrical force will dominate the printing and help achieve a stable cone-jet mode during the whole microgravity period, as shown in Figure 5c. The printing results in microgravity (printed during the flight) and a ground sample as reference (printed aboard the plane preflight) are shown in Figure 5d. Various line widths were achieved by varying the voltage and pulse frequency. On the ground, a pattern with a line width of 75.9 μm was able to be printed at a voltage of 1800 V and frequency of 100 Hz, while it was required to apply a higher voltage of 2200 V to achieve a similar line width (78.1 μm) in microgravity at the same frequency. This indicates that higher electrical field intensity is required to compensate for the lack of gravity to achieve a comparable line width. After annealing at 400 °C for 5 min, all printed patterns were highly conductive, with the resistances shown in Figure 5d. The high viscosity and stability of nanoinks helped stabilize them through the whole flight test, which also prevented the inks from drying too quickly when loaded in the printing nozzle. The morphology of printed silver nanoinks under zero gravity showed no significant difference from the samples printed on the ground (Figure S8). This proof-of-concept microgravity experiment proves the unique capability of EHD printing under zero-gravity conditions and opens a new venue for future on-demand manufacturing in space.

3. CONCLUSION

Using a biobased polymer HEC as a capping and stabilizing agent, doubled as a rheology modifier, silver nanoinks with various particle sizes and viscosities were synthesized. Compared with conventional silver nanoinks made from PVP, these HEC nanoinks are more economic and demonstrate long shelf life, high stability during printing, and excellent electrical conductivity upon sintering. In addition, the amount of HEC needed to obtain a good ink is as much as 20× less than a typical PVP synthesis, while the rate of the retention of HEC through the ink processing is over 60× higher. Ink properties such as particle size and viscosity are easily tunable by adjusting the sodium hydroxide and HEC content in the synthesis, respectively. Controlling the viscosity also provides an easy method to control the printing behavior when using EHD printing. The synthesized inks were found to be capable of being printed smoothly at feature sizes under 5 μm with a nozzle diameter of 100 μm, far outperforming commercially available alternatives. These attributes make this silver nanoink a strong candidate for use in EHD printing. In addition, a semiempirical model is presented that can be effectively used to predict printed line width based on ink properties and printer settings. Finally, the capability of EHD to print fine features and thin films in microgravity environments was confirmed through a parabolic flight test. This opens new opportunities for future in-space additive manufacturing of electronic devices.

4. EXPERIMENTAL SECTION

Materials. 2-Hydroxyethyl cellulose (90 000 g mol^{-1}), polyvinylpyrrolidone (55 000 g mol^{-1}), L-ascorbic acid (>99% purity), and Triton X-45 were purchased from Sigma-Aldrich. Silver nitrate, sodium hydroxide, and dimethyl sulfoxide (DMSO, >99.7% purity), and ethylene glycol were purchased from Fisher Scientific. Commercial silver ink 1 is product no. 796042 from Sigma-Aldrich. Commercial silver ink 2 is product no. JS-A191 from Novacentrix.

Ink Preparation. A stock solution of 7.5 M aqueous sodium hydroxide was prepared. For each sample, 3.00 g of silver nitrate was dissolved in 2 mL of DI water, and 1.50 g of L-ascorbic acid was dissolved in 7.5 mL of DI water. HEC with masses of 0.015, 0.020, and 0.030 g (for 20:1, 15:1, and 10:1 $AgNO_3$/HEC weight ratios, respectively) was dissolved in 15 mL of ethylene glycol under 500 rpm stirring at 100 °C. Once the HEC was fully dissolved, 0.40 mL of the sodium hydroxide stock solution was added, followed by the silver nitrate solution and then the L-ascorbic acid solution. The mixture was left to stir for 30 s. The resulting silver nanoparticle solution was washed with ethanol and acetone twice, and the particles were separated out through centrifugation. The particles were then suspended in 1.5 mL of DMSO, resulting in silver ink with 50 ± 1 wt % loading. Triton X-45 surfactant was added at 1.0 wt %.

SEM Imaging and Processing. An FEI Quanta 250 FE Scanning Electron Microscope was used to image the silver nanoparticles. Particle sizes were measured using ImageJ.

Conductivity Measurement. The inks were spin coated into thin films on plasma-treated 25 × 25 mm cover glass slides and left to air-dry overnight. The films were then sintered on hot plates at the specified temperatures for 30 min each. Sheet resistance measurements were taken using a Jandel RM2 4-point probe. The films were then cross-sectioned, and the cross-sectional thickness was measured by using SEM and ImageJ. Typical film thickness was approximately 1 μm. Resistivities were calculated by the following equation, where ρ is resistivity, V is voltage, I is current, and t is thickness:[40]

$$\rho = \frac{\pi}{\ln(2)} \frac{V}{I} t \tag{8}$$

Rheology Measurement. Rheology measurements were taken using an Anton Paar MCR 92 rheometer with a 25 mm 1° cone−plate setup with a gap dimension of 0.01 mm. For the viscosity measurements, 3 mL of silver nanoink was applied for each investigated ink. The shear rate was increased from 1 to 1000 s^{-1} over 5 min with a logarithmic selection.

Thermal Characterization. Small deposits of ink (0.05−0.10 g) were dried in an oven set to 70 °C. Thermogravimetric analysis was performed on the remaining solids using a Thermal Advantage TGA 5500. The samples as well as HEC powder were analyzed over a temperature range of 25 to 800 °C at a ramp of 20 °C per minute.

Printer Architecture. The EHD inkjet printer consists of an XYZ translating stage, positive and ground electrodes, glass micronozzle and syringe, signal generator, voltage amplifier, a high-speed camera, and a high intensity light source. The ink was loaded in the micronozzle and attached to the syringe and then mounted to the Z stage as an entity. The positive electrode was connected to the micronozzle and contacted the ink directly by using a metal conductor, and the ground was mounted under a glass substrate. The voltage signal was generated by the signal generator, amplified 1000 times by the amplifier, and then applied to the ink through the metal electrode. The printing process was monitored and recorded by a high-speed camera.

https://doi.org/10.1021/acsami.4c07592
ACS Appl. Mater. Interfaces XXXX, XXX, XXX−XXX

Printing Procedure. Before the printing, the ink was loaded to the syringe, and the micronozzle was rinsed with acetone to avoid clogging. A pressure regulator was connected to the syringe to control the back pressure for printing. Glass slides were precleaned with ethanol. The XY stages were leveled off to maintain a constant stand-off distance during the printing. The pulse signal was used to achieve better control of the droplet size and the jetting frequency for a precise control of the printing resolution. The high-speed camera was aligned to the nozzle tip to check the nozzle location and monitor the jetting status during the printing. The pattern was programed and would be finished automatically. After the printing, a post sintering step is required for the silver conductor.

Printing Model Validation. To validate the model derived to predict the printed line width, multiple printing experiments were performed with a focus on adjusting one operation parameter at a time and holding all others constant. These parameters included the back pressure, voltage amplitude, voltage frequency, duty ratio for pulse signals, plotting speed, and stand-off distance. To ensure stable printing in cone-jet mode and maximize the parameter range, a pretest was conducted to determine the appropriate range for each parameter. Subsequently, three printing tests were performed to model the effects of each parameter. Each test was repeated with three different inks to validate that the model works for solutions of varying viscosity and surface tension.

Zero-Gravity Experiments. Zero gravity experiments were performed through a parabolic flight test, which is capable of providing a zero-gravity atmosphere in 20-s bursts. The printer was mounted to the floor of the cabin of a specially modified Boeing 727 operated by parabolic flight company Zero-G. All equipment was fixed to the frame and plate of the printer to avoid floating at microgravity. The printing procedure is the same as the printing in the lab. In the experiment, 20 μL of 10:1 ink at 35 wt % solids loading was sonicated and preloaded to the nozzle tip with an inner diameter of 100 μm. A stand-off distance of 150 μm was chosen to avoid possible spraying and sputtering. A 100 mm × 75 mm × 1 mm glass slide was taped to the ground electrode. The printing speed was chosen between 2 mm s^{-1} and 3 mm s^{-1} to meet the requirement of 20-s-long microgravity duration depending on the overall length of different pattern designs. All patterns were printed with two layers to avoid accidental discontinuity due to the vibration of the airplane. The whole printing process was monitored by a high-speed camera with a frame rate of 60 fps, and the jetting process at microgravity was recorded using a frame rate of 10 000 fps.

■ ASSOCIATED CONTENT

Supporting Information

The Supporting Information is available free of charge at https://pubs.acs.org/doi/10.1021/acsami.4c07592.

AgNPs from 10× scaled up synthesis, nanoparticles of other materials synthesized with HEC, TGA curves for HEC and PVP powder, AgtNPs synthesized with PVP, resistance across HEC silver nanoink pattern printed and bent on polyimide, adhesion test of HEC silver nanoinks on polyimide, gravitational acceleration rate recorded during the parabolic flight test, SEM of HEC silver nanoinks printed in microgravity, properties of inks used for model validation, equation derivation (PDF)

■ AUTHOR INFORMATION

Corresponding Authors

Shan Jiang − *Department of Material Science and Engineering, Iowa State University, Ames, Iowa 50011, United States;* orcid.org/0000-0001-8119-9012; Email: sjiang1@iastate.edu

Hantang Qin − *Department of Industrial and Systems Engineering, University of Wisconsin—Madison, Madison, Wisconsin 53706, United States;* orcid.org/0000-0003-4180-7911; Email: hqin52@wisc.edu

Authors

Tyler Kirscht − *Department of Material Science and Engineering, Iowa State University, Ames, Iowa 50011, United States*

Liangkui Jiang − *Department of Industrial and Systems Engineering, University of Wisconsin—Madison, Madison, Wisconsin 53706, United States*

Fei Liu − *Department of Material Science and Engineering, Iowa State University, Ames, Iowa 50011, United States*

Xuepeng Jiang − *Department of Industrial and Systems Engineering, University of Wisconsin—Madison, Madison, Wisconsin 53706, United States*

Matthew Marander − *Department of Material Science and Engineering, Iowa State University, Ames, Iowa 50011, United States*

Ricardo Ortega − *Department of Material Science and Engineering, Iowa State University, Ames, Iowa 50011, United States*

Complete contact information is available at: https://pubs.acs.org/10.1021/acsami.4c07592

Notes

The authors declare the following competing financial interest(s): The patent application of the silver nano-ink for e-jet printing is currently under review for US Patent. Prof. Hantang Qin is the co-founder of a startup company with business interests of developing EHD printers. These activities are supported by an Innovation Corps Grant from the National Science Foundation.

■ ACKNOWLEDGMENTS

This project/material is based upon work supported by NASA Award No. 80NSSC21M0360, NASA Award No. 80MSFC23PA012, and the Iowa Space Grant Consortium under NASA Award No. 80NSSC20M0107.

■ REFERENCES

(1) Mkhize, N.; Bhaskaran, H. Electrohydrodynamic Jet Printing: Introductory Concepts and Considerations. *Small Sci.* **2022**, *2* (2), 2100073.

(2) Taylor, G. Electrically Driven Jets. *Proc. R. Soc. London* **1969**, *313* (1515), 453−475.

(3) Jiang, L.; Yu, L.; Premaratne, P.; Zhang, Z.; Qin, H. CFD-Based Numerical Modeling to Predict the Dimensions of Printed Droplets in Electrohydrodynamic Inkjet Printing. *J. Manuf. Process.* **2021**, *66*, 125−132.

(4) Park, J.-U.; Hardy, M.; Kang, S. J.; Barton, K.; Adair, K.; Mukhopadhyay, D. K.; Lee, C. Y.; Strano, M. S.; Alleyne, A. G.; Georgiadis, J. G.; Ferreira, P. M.; Rogers, J. A. High-Resolution Electrohydrodynamic Jet Printing. *Nat. Mater.* **2007**, *6* (10), 782−789.

(5) Guo, L.; Duan, Y.; Huang, Y.; Yin, Z. Experimental Study of the Influence of Ink Properties and Process Parameters on Ejection Volume in Electrohydrodynamic Jet Printing. *Micromachines (Basel)* **2018**, *9* (10), 522.

(6) Kwon, J.; Hong, S.; Suh, Y. D.; Yeo, J.; So, H.-M.; Chang, W. S.; Ko, S. H. Direct Micro Metal Patterning on Plastic Substrates by Electrohydrodynamic Jet Printing for Flexible Electronic Applications. *ECS J. Solid State Sci. Technol.* **2015**, *4* (4), P3052−P3056.

(7) Krainer, S.; Smit, C.; Hirn, U. The Effect of Viscosity and Surface Tension on Inkjet Printed Picoliter Dots. *RSC Adv.* **2019**, *9* (54), 31708−31719.

(8) Yang, J.; He, P.; Derby, B. Stability Bounds for Micron Scale Ag Conductor Lines Produced by Electrohydrodynamic Inkjet Printing. *ACS Appl. Mater. Interfaces* **2022**, *14* (34), 39601−39609.
(9) Kim, Y.; Jang, S.; Oh, J. H. High-Resolution Electrohydrodynamic Printing of Silver Nanoparticle Ink via Commercial Hypodermic Needles. *Appl. Phys. Lett.* **2015**, *106* (1), No. 014103.
(10) Ramon, A.; Liashenko, I.; Rosell-Llompart, J.; Cabot, A. On the Stability of Electrohydrodynamic Jet Printing Using Poly(Ethylene Oxide) Solvent-Based Inks. *Nanomaterials (Basel)* **2024**, *14* (3), 273.
(11) Nichols, R. K.; Carter, C. M.; Hood, J.-P.; Jackson, M. J.; Joseph, S. M. J.; Larson, H.; Lonstein, W. D.; Mai, R.; McCreight, R.; Mumm, H. C.; Oetken, M. L.; Pritchard, M. J.; Ryan, J. J. H.; Sincavage, S. E.; Slofer, W. *Space Systems: Emerging Technologies and Operations*; New Prairie Press, 2022.
(12) Qu, M.; Meng, Z.; Gao, T.; He, J.; Li, D. Exploration of Electrohydrodynamic Printing Potentially for In-Space Fabrication of Microscale Functional Structures: A Preliminary Study by an Anti-Gravity Configuration. *Addit. Manuf.* **2023**, *61*, No. 103349.
(13) Jiang, L.; Li, W.; Wolf, R.; Marander, M.; Kirscht, T.; Liu, F.; Jones, J. M.; Hill, C.; Jiang, S.; Qin, H. High-Sensitivity Fully Printed Flexible $BaTiO_3$-Based Capacitive Humidity Sensor for in-Space Manufacturing by Electrohydrodynamic Inkjet Printing. *IEEE Sens. J.* **2024**, 1.
(14) Tan, H. W.; An, J.; Chua, C. K.; Tran, T. Metallic Nanoparticle Inks for 3D Printing of Electronics. *Adv. Electron. Mater.* **2019**, *5* (5), 1800831.
(15) Ding, J.; Liu, J.; Tian, Q.; Wu, Z.; Yao, W.; Dai, Z.; Liu, L.; Wu, W. Preparing of Highly Conductive Patterns on Flexible Substrates by Screen Printing of Silver Nanoparticles with Different Size Distribution. *Nanoscale Res. Lett.* **2016**, *11* (1), 412.
(16) Zhao, C.-F.; Wang, J.; Zhang, Z.-Q.; Sun, Z.; Maimaitimin, Z. Silver-based Conductive Ink on Paper Electrodes Based on Micro-pen Writing for Electroanalytical Applications. *ChemElectroChem.* **2022**, *9* (21), No. e202200948.
(17) Shang, Y.; Sun, Q.; Lu, Y.; Tang, C.; Zuo, C.; Yan, B. Improvement of Electrical and Mechanical Properties of Printed Silver Wire by Adjusting Particle Size Distribution of Multiscale Silver Nanoparticle Ink. *J. Electron. Mater.* **2022**, *51* (11), 6503−6511.
(18) Fernandes, I. J.; Aroche, A. F.; Schuck, A.; Lamberty, P.; Peter, C. R.; Hasenkamp, W.; Rocha, T. L. A. C. Silver Nanoparticle Conductive Inks: Synthesis, Characterization, and Fabrication of Inkjet-Printed Flexible Electrodes. *Sci. Rep.* **2020**, *10* (1), 8878.
(19) Kant, T.; Shrivas, K.; Ganesan, V.; Mahipal, Y. K.; Devi, R.; Deb, M. K.; Shankar, R. Flexible Printed Paper Electrode with Silver Nano-Ink for Electrochemical Applications. *Microchem. J.* **2020**, *155*, 104687.
(20) Zhuo, L.; Liu, W.; Zhao, Z.; Yin, E.; Li, C.; Zhou, L.; Zhang, Q.; Feng, Y.; Lin, S. Cost-Effective Silver Nano-Ink for Inkjet Printing in Application of Flexible Electronic Devices. *Chem. Phys. Lett.* **2020**, *757*, 137904.
(21) Cao, L.; Bai, X.; Lin, Z.; Zhang, P.; Deng, S.; Du, X.; Li, W. The Preparation of Ag Nanoparticle and Ink Used for Inkjet Printing of Paper Based Conductive Patterns. *Materials (Basel)* **2017**, *10* (9), 1004.
(22) Peng, P.; Li, L.; Guo, W.; Hui, Z.; Fu, J.; Jin, C.; Liu, Y.; Zhu, Y. Room-Temperature Joining of Silver Nanoparticles Using Potassium Chloride Solution for Flexible Electrode Application. *J. Phys. Chem. C Nanomater. Interfaces* **2018**, *122* (5), 2704−2711.
(23) Zhang, Z.; Zhang, X.; Xin, Z.; Deng, M.; Wen, Y.; Song, Y. Synthesis of Monodisperse Silver Nanoparticles for Ink-Jet Printed Flexible Electronics. *Nanotechnology* **2011**, *22* (42), No. 425601.
(24) Naik, S. C.; Pittman, J. F. T.; Richardson, J. F.; Lansdown, A. R. Evaluation of Hydroxyethyl Cellulose Ether as a Thickener for Aqueous Lubricants or Hydraulic Fluids. *Wear* **1978**, *50* (1), 155−168.
(25) Maestro, A.; González, C.; Gutiérrez, J. M. Rheological Behavior of Hydrophobically Modified Hydroxyethyl Cellulose Solutions: A Linear Viscoelastic Model. *J. Rheol. (N. Y. N. Y.)* **2002**, *46* (1), 127−143.
(26) Benyounes, K.; Remli, S.; Benmounah, A. Rheological Behavior of Hydroxyethylcellulose (HEC) Solutions. *J. Phys. Conf. Ser.* **2018**, *1045*, No. 012008.
(27) El-Sheikh, M. A.; El-Rafie, S. M.; Abdel-Halim, E. S.; El-Rafie, M. H. Green Synthesis of Hydroxyethyl Cellulose-Stabilized Silver Nanoparticles. *J. Polym.* **2013**, *2013*, 1−11.
(28) Zulkifli, F. H.; Hussain, F. S. J.; Zeyohannes, S. S.; Rasad, M. S. B. A.; Yusuff, M. M. A Facile Synthesis Method of Hydroxyethyl Cellulose-Silver Nanoparticle Scaffolds for Skin Tissue Engineering Applications. *Mater. Sci. Eng. C Mater. Biol. Appl.* **2017**, *79*, 151−160.
(29) Qin, Y.; Ji, X.; Jing, J.; Liu, H.; Wu, H.; Yang, W. Size Control over Spherical Silver Nanoparticles by Ascorbic Acid Reduction. *Colloids Surf. A Physicochem. Eng. Asp.* **2010**, *372* (1−3), 172−176.
(30) Wünscher, S.; Abbel, R.; Perelaer, J.; Schubert, U. S. Progress of Alternative Sintering Approaches of Inkjet-Printed Metal Inks and Their Application for Manufacturing of Flexible Electronic Devices. *J. Mater. Chem. C Mater. Opt. Electron. Devices* **2014**, *2* (48), 10232−10261.
(31) Bae, J.; Lee, J.; Hyun Kim, S. Effects of Polymer Properties on Jetting Performance of Electrohydrodynamic Printing. *J. Appl. Polym. Sci.* **2017**, *134* (35), 45044.
(32) Saville, D. A. Electrohydrodynamics: The Taylor-Melcher Leaky Dielectric Model. *Annu. Rev. Fluid Mech.* **1997**, *29* (1), 27−64.
(33) Chen, C.-H.; Saville, D. A.; Aksay, I. A. Scaling Laws for Pulsed Electrohydrodynamic Drop Formation. *Appl. Phys. Lett.* **2006**, *89* (12), 124103.
(34) Choi, H. K.; Park, J.-U.; Park, O. O.; Ferreira, P. M.; Georgiadis, J. G.; Rogers, J. A. Scaling Laws for Jet Pulsations Associated with High-Resolution Electrohydrodynamic Printing. *Appl. Phys. Lett.* **2008**, *92* (12), 123109.
(35) Batchelor, G. K. *An Introduction to Fluid Dynamics*; Cambridge University Press: Cambridge, England, 1967.
(36) Marginean, I.; Nemes, P.; Vertes, A. Order-Chaos-Order Transitions in Electrosprays: The Electrified Dripping Faucet. *Phys. Rev. Lett.* **2006**, *97* (6), No. 064502.
(37) Stringer, J.; Derby, B. Formation and Stability of Lines Produced by Inkjet Printing. *Langmuir* **2010**, *26* (12), 10365−10372.
(38) Prater, T.; Edmunson, J.; Fiske, M.; Ledbetter, F.; Hill, C.; Meyyappan, M.; Roberts, C.; Huebner, L.; Hall, P.; Werkheiser, N. *NASA's in-Space Manufacturing Project: Update on Manufacturing Technologies and Materials to Enable More Sustainable and Safer Exploration*; 2019.
(39) Murali, H.; Bell, J.; Cheng, Q.; Mairena, K.; Centeno, E.; Durgin, G. D.; Shi, E. Using Inkjet Printed Circuits on a Transparent Substrate for Microwave Energy Harvesting for Space Based Solar Power. In *2017 IEEE International Conference on Wireless for Space and Extreme Environments (WiSEE)*; IEEE, 2017; pp 140−143.
(40) Smits, F. M. Measurement of Sheet Resistivities with the Four-Point Probe. *Bell Syst. Technol. J.* **1958**, *37* (3), 711−718.

https://doi.org/10.1021/acsami.4c07592
ACS Appl. Mater. Interfaces XXXX, XXX, XXX−XXX